Contents lists available at ScienceDirect

Arabian Journal of Chemistry

journal homepage: www.ksu.edu.sa

Fe-Ni bimetallic supported on mordenite catalyst for selective oxidation of veratryl alcohol in a continuous reactor

N. Gayathri [a], P. Tamizhdurai [a,*], C. Kavitha [a], V.L. Mangesh [b,*], P. Santhana Krishnan [c], A. Vijayaraj [a], R. Kumaran [a], Nadavala Siva Kumar [d], Ahmed S. Al-Fatesh [d], Salwa B. Alreshaidan [e]

[a] Department of Chemistry, Dwaraka Doss Goverdhan Doss Vaishnav College (Autonomous) (Affiliated to the University of Madras, Chennai), 833, Gokul Bagh, E.V.R. Periyar Road, Arumbakkam, Chennai 600 106, Tamil Nadu, India
[b] Department of Marine Engineering, Indian Maritime University, Chennai 600119, India
[c] Department of Chemistry, Pukyong National University, Busan 48513, Republic of Korea
[d] Department of Chemical Engineering, College of Engineering, King Saud University, P.O. Box 800, Riyadh 11421, Saudi Arabia
[e] Department of Chemistry, Faculty of Science, King Saud University, P.O. Box 800, Riyadh 11451, Saudi Arabia

ARTICLE INFO

Keywords:
Mordenite
Veratryl alcohol (VA)
Selective oxidation
Continuous reactor
Veratraldehyde (VADE)

ABSTRACT

Veratryl alcohol (VA) is preferentially oxidized to veratraldehyde (VADE) using a heterogeneous catalyst, which is more favoured in industries. Commercial mordenite (Ca,Na_2,K_2) $Al_2Si_{10}O_{24}{\cdot}7H_2O$) was desilicated with NaOH and loaded with nickel and iron bimetal by the wet impregnation method. The synthesised Mordenite-Fe(5 %)/Ni (5–20 %) bimetallic catalyst, possessing active Bronsted acid sites, was employed to selectively oxidize the veratryl alcohol reaction. FT-IR, XRD, BET, HR-SEM, HR-TEM, and TPD were employed to determine the catalyst's textural attributes, morphology, chemical properties, and stability. Selective oxidation was performed over the catalysts using TBHP as an oxidant in a continuous reactor. To examine the most active catalyst among the four and to maximise the conversion and yield, the reaction conditions are optimised for various reaction parameters The reaction conditions were optimized by attaining 100 % conversion at temperature (90° C) for time (2 hr) and a maximum conversion of 97 % and a selectivity of 99 % at 10 bar pressure, WHSV (1.0 h^{-1}) with acetonitrile solvent. The result of the study display that Fe (5 %) and Ni(15 %) impregnated on mordenite exhibits excellent catalytic stability with conversion (100 %) and selectivity (99 %) among the other catalysts. During regeneration, the conversion rate declined from 99.5 to 92.4.7 % and selectivity declined from 100 % to 96.2 % at the end of the seventh cycle. The high selectivity and stability of MOR-Fe(5 %)/Ni(15 %) imply that they might function properly as appropriate catalysts for the oxidation of aromatic alcohols. The advantages of the current synthesis are its cost-efficiency and eco-friendliness.

1. Introduction

In recent years, much emphasis has been placed on the catalytic conversion of lignocelluloses into high-value-added products and biofuels (Upham et al., 2021). Cellulose, hemicellulose, and lignin constitute the majority of the ample and inexhaustible resources known as lingo cellulosic biomass (Güngör and Özen, 2021; Liu et al., 2021). A significant quantity of lignin is produced as a waste product from the pulp and paper industry's cellulose extraction and is burned to produce energy (Bogdanov et al., 2021; Wang et al., 2021). The only source of aromatics in nature is lignin. Lignin is a polymer with a three-dimensional structure of methoxylated phenyl propane. Sinapyl alcohol, coniferyl alcohol, and p-coumaryl alcohol are its three monomers. Most of the links in lignin are ether bonds, but there are also some C—C bonds (Li et al., 2020; Wang et al., 2020; Liu et al., 2020). The carbon atoms in the aliphatic side chains are denoted as α, β, γ, and those in the aromatic moieties as 1 to 6 (Sheng et al., 2020). These designations are used to classify the linkages between two mono lignols. The most prevalent linkage between the lignin structural block is O-4. Lignin vaporisation involves the cleavage of lignin structure into phenolic building blocks, which can be further converted into the desired product (Al-Mamoori et al., 2020). In biorefinery research, lignin valorisation is

* Corresponding authors.
E-mail addresses: tamizhvkt2010@gmail.com (P. Tamizhdurai), vlmangesh@gmail.com (V.L. Mangesh).

https://doi.org/10.1016/j.arabjc.2023.105506
Received 19 September 2023; Accepted 28 November 2023
Available online 30 November 2023

one of the foremost conversions of lignin into high-value-added chemicals (Kozin et al., 2020; Nie et al., 2020; Liu et al., 2020; Sakthinathan et al., 2020; Tamizhdurai et al., 2019). The suitable process for vaporizing lignin and lignin model compounds is oxidative depolymerisation using oxidants like oxygen or hydrogen peroxide (H_2O_2) (Zhao et al., 2021; Sahu et al., 2019; Neethu et al., 2021).

The investigation of catalysts supported by Iron (Fe) and copper (Cu) has been conducted to explore their efficacy in the selective catalytic oxidation of benzyl alcohol and the coupling of carbon–carbon (C—C) bonds (Das et al., 2020; Baruah et al., 2021; Gogoi et al., 2021). The catalyst prepared with a nickel-to-iron molar ratio of 2: 1 exhibited a good hydrotalcite structure and moderate catalytic activity for the hydrotreatment of anisole (Aswin et al., 2022).

Oxidation of VA to VADE is the reaction that represents the oxidative cleavage of β-O-4 (Santhana Krishnan et al., 2019). Veratryl alcohol is the model substrate of lignin. Veratraldehyde is employed as an odorant and flavouring agent. Due to its woodsy scent, it is well-liked commercially (Ibrahim et al., 2021; Ishimori et al., 2020; KaiyuLi and Guilian, 2022; Liu et al., 2021). It is also used as an intermediate in the synthesis of pharmaceutical drugs and in the synthesis of drugs for angiocardiography (Arumugam et al., 2019; Sun and Gao, 2020). Veratraldehyde is typically made by methylating vanillin with crude oil. However, industries spend more on bio-based veratraldehyde than on veratraldehyde made from crude oil (Chen et al., 2020). One of the key processes in the formulation of chemical agents, perfumes, flavorings, medicines, and compounds with biological activity is the selective oxidation of alcohol to its equivalent aldehyde or keto group (Liu et al., 2021; Lorenzo et al., 2022; Melián-Rodríguez et al., 2015; Gillet et al., 2017; Vangeel et al., 2020; Wu et al., 2015). During a selective oxidation reaction, environmentally friendly oxidants such as O_2, H_2O_2, etc., are used as stoichiometric oxidants because they produce water as a by-product (Dhinagaran et al., 2022; Larson et al., 2013; Kervinen et al., 2002). Strong stoichiometric oxidants are not preferred because they produce hazardous wastes. Oxidation reactions using homogeneous catalysts are studied; the conversion and yield were good, but the recovery and recycling of the catalyst were difficult. Hence heterogeneous catalysts were considered for the selective oxidation of biomass-derived substrates (Liu, 2020; Fan et al., 2014; Wu et al., 2016; Paixão et al., 2010).

Larson has studied the oxidation of VA to VADE by a mediator enzyme laccase, which yields 94 % of veratraldehyde. Though the yield was good for the enzymatic conversion of lignin and lignin exemplary compounds, some drawbacks exist, e.g., poor thermal stability, enzyme deactivation, etc.. (Ivanova et al., 2014). Kervinen described the oxidation of VA to VADE in a homogeneous condition; cobalt salen complexes are employed as a catalyst with O_2 as an oxidant; the conversion was 100 %, but it wasn't easy to recover and reuse the catalyst (Narayanan et al., 2015; Stefanidis et al., 2013; Aloise et al., 2020; Thommes et al., 2015). Mate reported the oxidation of VA to VADE by heterogeneous catalyst CO_3O_4 using O_2 as an oxidant at 413 K; the selectivity was good at 96 %, and the catalyst was also recovered and reused, but the conversion was only 85 % (Li et al., 2009; Sabarish and Unnikrishnan, 2019; Tamizhdurai et al., 2022; Weng et al., 2015). Fan et al. reported the aerobic oxidation of VA to VADE using combined ruthenium imidazole and CuO ionic liquid as catalysts (130), and the yield was up to 95 %. However, the reusability of the catalyst was not documented (Zakzeski et al., 2010; Sheng et al., 2019; Santhana Krishnan et al., 2017). *Wu* and co-workers reported the oxidation of veratryl alcohol to veratraldehyde using a composite catalyst, Au/GQDs/Fe_3O_4 at 100; the conversion was up to 90 %, and the catalytic action was amplified by adding the base K_2CO_3 (Tamizhdurai et al., 2018). Dhinagaran reported the selective oxidation of VA to VADE by employing SBA-15-supported CuO as a catalyst and tertiary butyl hydroperoxide as an oxidant, the conversion was equal to 82 % at 80, and the catalyst was recycled and reused (Krishnan et al., 2019). Synergistic effects and additional active sites make bimetallic catalysts more active than monometallic ones. Secondary metals prevent primary metals from sintering or leaching, extending catalyst lifetime. Bimetallic catalysts are more practical for industrial operations because they may be recycled and reused without losing activity or selectivity and reduce pollution by operating at lower temperatures and pressures (Khan et al., 2023). The literature also reports on the hazardous nature of pollutants such as methanol and naproxen, as well as the effective methods for their removal (Kamyab et al., 2022; Jangjou et al., 2023).

In this work, the selective oxidation of VA to VADE was done by employing the bimetals impregnated on Mordenite catalyst MOR-Fe/Ni. Mordenite is a type of zeolite. Mordenite has a one-dimensional pore system and high silicon content. Because of its two-dimensional porous structure, mordenite had very little reactant molecule diffusion. To increase the porosity in mordenite, a desilication process is performed. The desilicated mordenite was impregnated by a metal Fe-5 %, and the second metal loading was varied by different percentages of Ni (5–20 %). The reaction was carried out using H_2O_2 as an oxidant, and the conditions were optimised for the selective formation of veratraldehyde. The general reaction of selective oxidation of veratryl alcohol is shown in Fig. 1.

2. Experimental method

2.1. Materials

The chemicals bought were of the analytical reagent (AR, 99 %) grade and didn't need to be further purified·H_2O_2, sodium hydroxide, ammonium nitrate, and veratryl alcohol were purchased from Sigma Aldrich (98 %). Aqueous *tert*-butyl hydroperoxide (TBHP), dichloromethane (DCM), N, N-dimethylformamide (DFM), chloroform ($CHCl_3$), and acetonitrile were purchased from Rankem (100 %). Nickel hexachloride and ferrous heptasulphate were purchased from Merck Chemicals (99 %).

2.2. Alkaline treatment of mordenite

The commercial mordenite sample underwent a 5 h calcination process in dry air at 550 °C. A mordenite sample was desilicated using sodium hydroxide as a desilicating agent. The MOR sample was stirred in a 0.2 M NaOH solution, and the temperature was maintained at 70 °C for 2 h. The sample that had been alkaline-treated was then completely filtered, washed, and had its pH maintained at 7 before being dried at 90 °C overnight and then calcined at 550 °C for 5 h. Exchanges with a 2 M NH_4NO_3 solution transformed the alkaline-treated material into the protonic state. The exchanges were carried out for about 3 h, and the temperature was maintained at 80 °C. It was filtered and washed thoroughly, and the solids were dried overnight at 90 °C, and the solids were calcined at 550 °C. for 5 h (Vu et al., 2016). The base alteration dramatically enhances the mesoporous surface area of H-mordenite (Koshti and Bandyopadhyay, 2023).

2.3. Impregnation of Fe on mordenite zeolite

The wet impregnation approach was espoused for Fe impregnation. The wet mordenite sample was subjected to stirring for a duration of 2 h at a 500 rpm. The loading of iron was determined to be 5 wt%. The metal is bound to the mesoporous site of the mordenite. The samples were dried at 100 °C overnight. The desiccated sample was calcined for 3 h at 550 °C. The substance was grounded into fine powder.

2.4. Impregnation of Ni metal on mordenite

In the Fe-impregnated mordenite sample, another metal was also loaded by the wet impregnation method. Nickel chloride was used as a metal precursor. wt. % loading of Ni was varied by 5–20 %, yielding four different samples. The calculated amount (5 %, 10 %, 15 %, 20 %) of

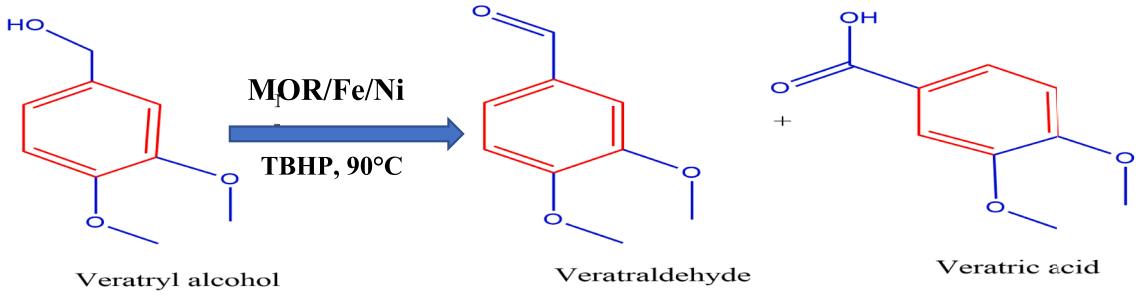

Fig. 1. Selective oxidation of veratryl alcohol.

nickel with the mordenite sample in wet condition was stirred for 2 h at 500 rpm. The four samples were calcined at 550 °C for 3 h after being desiccated overnight at 100 °C.

2.5. Description of the reactor Setup

The experiments were performed in a fixed bed high-pressure stainless steel reactor with a 6 mm internal diameter in a downflow condition. 3.2 g of the catalyst (size 1–2 mm) was typically used, undiluted. The high-pressure fixed-bed micro-reactor used in this investigation is represented schematically in Fig. S1. There are three sections in the flow diagram: The first part (right side in the Figure) contains the feed input lines; the second section (middle section) contains the reactor and the eight-port valve; and the third section (left side in the Figure) contains the product condenser and vent. The first section consists of feed line filters, check valves, and mass flow controls that govern gas flow. A pump feeds the liquid reactant through a second input connection located next to the gas lines and into an eight-port valve and the reactor. The feed mixture can be pumped into the reactor from the hot oven in the centre through an eight-port valve. This also allows injecting the vaporised feed combination or product into an online gas chromatograph. The temperature indicator and controller measure the catalyst bed temperature and regulate the reactor furnace temperature. A mass flow controller is used to regulate and measure the oven temperature, which is typically kept at 90 °C. PG indicates the pressure inside the reactor. The last section includes the drain valve, liquid condenser, high-pressure separator, and back pressure regulator.

2.6. Catalytic activity studies

The reactions were performed in a 6 mm inner diameter down-flow mode fixed bed stainless steel high-pressure reactor. The catalyst (size 1–2 mm) was loaded and dried in CO_2-free air for 6 h at 250 °C. At constant pressure, the reactor was heated ranging from 60 to 110 °C for 1 h. When the airflow, temperature, and pressure were tuned to the required values, the feed was then injected. The reactions occurred at temperatures between 60 and 100 °C, under 10 bar pressure, with 3.2 g of catalyst loaded and WHSV (h^{-1}). In the propylene glycol example, the free air (CO_2 free)/feed (mole ratio) was 2 (solvent comprising 25 mmol of aqueous *tert*-butyl hydroperoxide (TBHP) and 20 mmol of propylene glycol). The output components were evaluated in a GC equipped with an FID (flame ionisation detector) using N_2 carrier gas in an SGE BPX70 capillary column.

Calculating the conversion and selectivity by using the following relations

$$\text{Conversion } (\%) = 100 \times [VA]^0 - [VA]^t/[VA]^0 \quad (1)$$

$[VA]^0$ = Veratryl Alcohol Initial concentration
$[VA]^t$ = Time of the Veratryl Alcohol concentration

$$\text{Selectivity } (\%) = \frac{\text{moles of individual product}}{\text{moles of total products}} \times 100 \quad (2)$$

2.7. Catalyst characterization

Several physicochemical approaches, including high-angle XRD, N_2 physisorption tests, and temperature-programmed desorption, were used to characterize all the produced catalysts (TPD). A BRUCKER D8 diffractometer was used to acquire the diffraction pattern of the supports and catalysts at a sharp angle of 10–80° using Cu Kα radiation (=1.548). At the temperature of liquid N_2, the QUADRASORB SI automated analyzer detected N_2 sorption isotherms. To prepare the sample for analysis, 30 mg was degassed with N_2 flow at 300 °C for 4 h. The BET technique determined the precise values of the surface areas of the supports and catalysts. The BJH method was used to derive the pore size distribution graph from the desorption isotherms, and N_2 adsorption was employed to calculate the pore volume (Vp) at a relative pressure range of 0.98. With the Micrometrics chemisorbs 2750 TPD and gas combinations of 10 % NH_3/90 % He and 5 % H_2/95 % Ar, respectively, temperature-programmed desorption tests were conducted. Before analysis, 30 mg of the substance was degassed for three hours at 200 °C with N2 gas flow. Before performing the TPD analysis, 0.03 g of the sample was treated at 350 °C for two hours with helium gas flow (30 cm^3/min) to remove the physisorbed moisture. The NH_3/He gas combination was set to adsorb on these samples for 30–40 min (50 cm^3/min). For 60 min, helium gas was circulated over the catalyst at a rate of 30 cm^3/min to remove the physisorbed NH_3 accumulated on the sample surface. The TPD profile was then captured by gradually raising the temperature by 10 °C/min from 100 °C to 600 °C. The amount of NH_3 consumed helped identify the acid sites. Utilizing a PerkinElmer FT-IR C101375 Spectrophotometer, the FT-IR spectrum was carried out. The KBr pellet technique was used to prepare the samples.

3. Results and discussion

3.1. X-ray diffraction studies

Fig. 2 illustrates the high-angle powder XRD patterns for the various molar concentrations of MOR-Fe/Ni catalysts. The four samples confirm the expected diffraction peaks of mordenite-type zeolites. It exhibits diffraction peaks peculiar to mordenite at 2θ = values comparable to 6.54°, 8.76°, 9.78°, 13.56°, 15.30°, 19.74°, 22.40°, 25.8°, 26.43°, and 31.06°. The diffraction patterns are indeed connected to the [1 1 0], [0 2 0], [2 0 0], [1 1 1], [3 1 0], [3 3 0], [1 5 0], [2 0 2], [3 5 0], [1 3 2], and [4 0 2] planes. According to prior studies, the diffraction maxima of all the dealuminated samples could be precisely associated with the orthorhombic phase of the mordenite structure, which correlates to the JCPDS data; card No.: 43–0171. The relative crystalline of the samples was evaluated by analysing the peak area beneath the diffraction maxima 2θ at 9.8°, 13.5°, and 26.4°, and the XRD patterns of these samples was also studied over a 2θ range of 5–30° using MDI-Jade 6.5 software. The crystalline phase corresponding to the MOR zeolite structure (JCPDS card 011–0155) was validated based on the positions of the characteristic lines obtained from the JCPDS card; the lines at 44.5°,

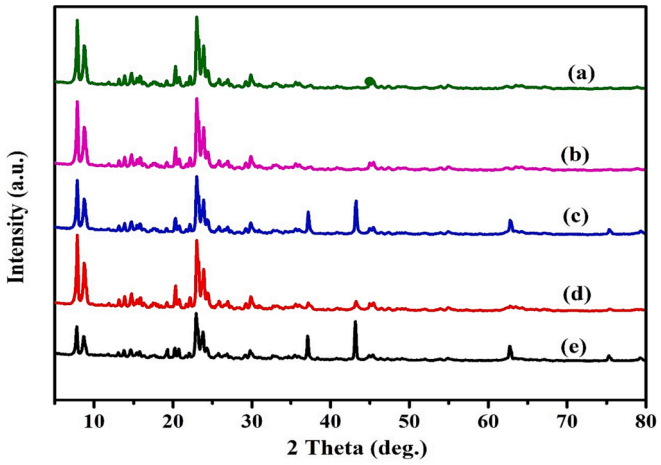

Fig. 2. X-ray difffraction patterns of a) Pure Mordenite b) MOR-Fe(5%)/Ni (5%), c) MOR-Fe(5%)/Ni(10%), d)) MOR-Fe(5%)/Ni(15%), e) MOR-Fe(5%)/Ni(20%).

62.8°, and 76.4° correspond to nickel crystallites (111), (200), and (220). Furthermore, three main species, $FeNi_3$, NiO, and $Ni(Fe)Fe_2O_4$, were reported in the samples calcined at 773 K with various Fe/Ni ratios. The peak intensities of both NiO and $FeNi_3$ increased with raising Ni concentration, revealing that the increase in Ni content facilitated the formation of the $FeNi_3$ alloy. As compared to this, the peak intensity of the $Ni(Fe)Fe_2O_4$ phase was relatively consistent throughout. The oxygen deficit of $Ni(Fe)$-Fe_2O_4 may have been progressively penetrated by air (samples were calcined in an environment of air.), stabilising the structure of $Ni(Fe)Fe_2O_4$ (Verboekend et al., 2013).

3.2. FT-IR spectra analysis

The vibration of different bonds that indicate the presence of desilicated mordenite has been explored using FT-IR spectroscopy. The FT-IR absorbance bands for various wt. % of the MOR-Fe/Ni catalyst are depicted in Fig. 3. The absorption bands of the mordenite sample were inferred at 3518, 3384, 1631, 1223, 1050–1150, 800, 590, 547, 470, and 433 cm^{-1} (Verboekend and Pérez-Ramírez, 2011). The spectra of the four distinct samples are indistinguishable, which is apparent in Fig. 3.

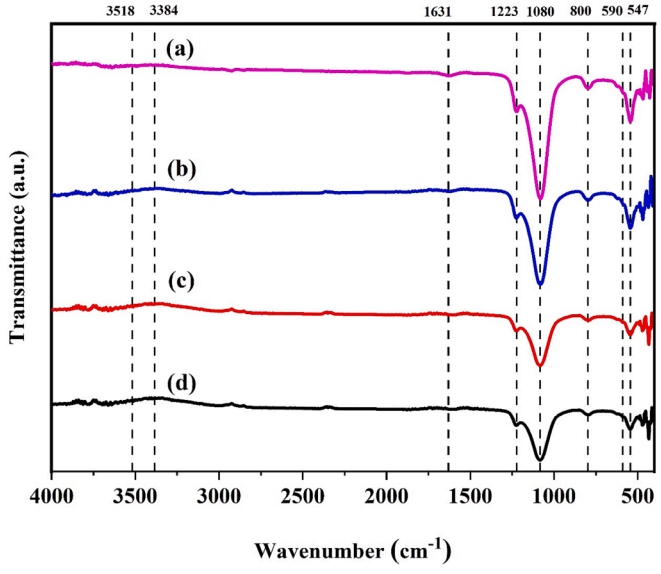

Fig. 3. FT-IR spectra of a) MOR-Fe(5%)/Ni(5%), b)) MOR-Fe(5%)/Ni(10%), c)) MOR-Fe(5%)/Ni(15%), d)) MOR-Fe(5%)/Ni(20%) samples.

With an upsurge in the Ni metal loading, the peak intensity declined. The decline in intensity exemplifies that the Ni metal is adsorbed on the surface. The external and internal symmetric stretching vibration, exterior and internal asymmetric stretching vibration, and T-O bending vibration are the reasons for the absorption spectrum at 433, 470, 547, 590, 800, 1080, and 1223 cm^{-1}. The water molecule's bending vibration induces the absorption maxima at 1631 cm^{-1}. Water molecules in the zeolite structure begin to bend and vibrate due to water being absorbed by the samples during compression with KB. The detached silanol groups (Si—O—H) and the stretched water molecules adsorbed on the surface of the samples both contribute to the bands at 3518 and 3384 cm^{-1}. The vibration of the Si—O—Si bond attained a broad peak above 1000 cm^{-1}, and the bending vibration occurred at 800 cm^{-1}. Tetrahedral SiO_4 and AlO_4 units form the double five-ring (D5R) structure associated with the vibration band at 590 cm^{-1} (Cao et al., 2021; Molleti and Yadav, 2017). Even after thorough desilication with alkaline treatment, the mordenite structure persists.

3.3. N_2 adsorption/desorption isotherms (BET)

The textural characteristics of the catalysts are expressed in Table 1, and Fig. 4 exhibits the nitrogen adsorption and desorption isotherms of MOR-Fe/Ni catalysts. A type IV isotherm with an evident H4-type hysteresis loop is visible in the alkaline-treated, bimetal-loaded mordenite. Mesopores were present in all of the samples, as asserted by the hysteresis loop, which was in the range of 0.45 and 0.95P/P_0. As can be seen in Table 1, the surface area shrinks as the second metal is loaded quite heavily. However, compared to the other cases, the MOR-Fe (5 %) and Ni (5 %) have a more extensive surface. It is apparent from Table 1 that as the loading of Ni increases, the external surface area tends to increase from 51 to 56 m^2/g. Mesopores in the crystallite primarily contribute to the increase in external surface area. Additionally, the overall pore volume improves from 0.29 to 0.31 cm^3/g. The MOR-Fe (5 %), Ni (20 %), and combined samples' total pore volume and microporous properties declined, primarily attributable to the blocking of the mordenite pore structure brought on by excessive metal loading. However, further increases in the metal loading result in a massive decrease in the pore volume and microporous surface area but no perceptible change in the mesopores volume (Yu et al., 2022).

3.4. High resolution-scanning electron microscopy (HR-SEM)

The dimensions and morphology of the samples have been predicted using a scanning electron microscope. Fig. 5 illustrates the SEM images of desilicated mordenite samples. Mesopores are vividly apparent in the SEM image. The various weight concentrations of MOR-Fe/Ni catalysts have different morphologies based on the size and shape of the particles. After the alkaline treatment of mordenite, cracking occurs, and roughness is created. The rough surface is produced by mesopores development in the alkaline-treated mordenite. The mordenite is composed of nanoparticles that construct its micro blocks (Ma et al., 2016; Wahono et al., 2019; McCusker and Baerlocher, 2007; Sánchez-López et al., 2019; Sánchez-López et al., 2022). The voids are aggregated with the mordenite nanoparticles. Less aggregation can be seen in the desilicated mordenite. This affirms that the desilication induced by the alkaline treatment impacts the particle size and shape of the mordenite (Kooyman, 2008). The particle size of the MOR-Fe/Ni bimetallic catalyst may vary because of the adsorption of various concentrations of the metal. Fig. 5(a) shows the development of stacked, multi-layered sheets of mordenite, a random deposition of Ni metal over the surface, and then the incorporation of Fe (5 %), leading to the multi-layered sheets of mordenite being covered by the active metals and the surface being obscured. Fig. 5(b) depict that an increase in the amount of metal incorporation leads to accumulation on the surface of the mordenite and changes in the morphology. Fig. 5(c) exhibits that the particle becomes denser, and even some particles are agglomerated. The reduction in size

Table 1
Textural characteristics of Cu/Ni and supported H-Beta Catalysts.

Catalyst Entry	Surface area (m^2/g)	S micro-(m^2/g)	S ext(m^2/g)	V total (cm^3/g)	V micro (cm^3/g)	Vmeso (Cm^3/g)	Acidity (mmol/g)2 Total[c]	*LT peak[c]	*HT Peak[c]
MOR-Fe(5 %)/Ni (5)	396	345	51	0.296	0.208	0.088	1.38	0.70	0.68
MOR-Fe(5 %)/Ni (10)	388	335	53	0.310	0.219	0.091	1.45	0.76	0.69
MOR-Fe(5 %)/Ni (15)	380	326	54	0.316	0.213	0.103	1.78	0.78	0.99
MOR-Fe(5 %)/Ni (20)	376	320	56	0.289	0.180	0.109	1.65	0.76	0.89

[a]Measured by the t-plot method. [b]Vmeso = VTotal-Vmicro. [c]Total acidity was determined by the standard temperature-programmed desorption of ammonia (TPDA) method.*LT = Low Temperature, *HT = High temperature.

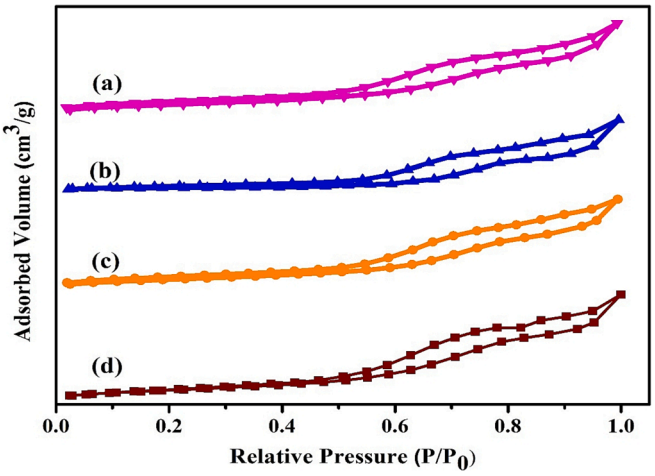

Fig. 4. N_2 adsorption isotherm(BET) of a) MOR-Fe(5%)/Ni(5%), b) MOR Fe (5%)/Ni(10%), c)) MOR-Fe(5%)/Ni(15%), d)) MOR-Fe(5%)/Ni(20%) samples.

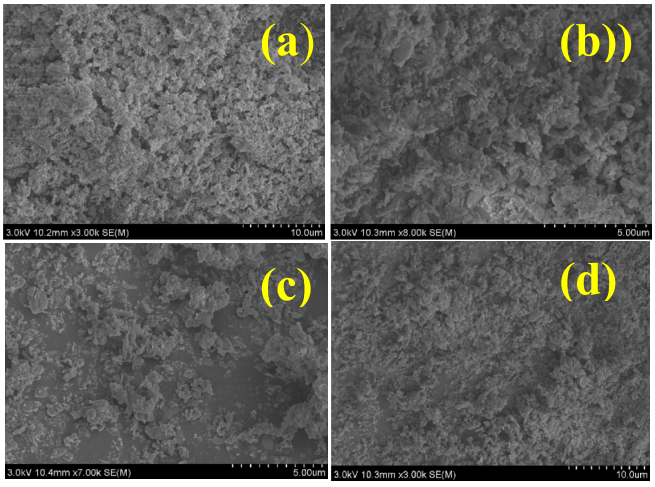

Fig. 5. High Resolution-Scanning Electron Microscopy (HR-SEM) of a) MOR-Fe (5%)/Ni(5%), b) MOR-Fe(5%)/Ni(10%), c) MOR-Fe(5%)/Ni(15%), d) MOR-Fe (5%)/Ni(20%) samples.

inside the catalyst is due to the distortion produced by the nickel atoms, which are shown in Fig. 4(d) demonstrates a less crystalline structure, because it is due to the stress development of the catalyst at higher loadings of different compositions.

3.5. High-resolution transmission electron microscopy (HR-TEM)

The size, morphology, and dispersion of active metals are determined using high-resolution transmission electron microscopy. HR-TEM micrographs of Ni (5–20 wt%) and Fe (5 wt%) impregnated on mordenite samples are shown in Fig. 6(a–d). The alkaline-treated mordenite greatly influences the change in size and structure. Fig. 6(a–d) shows the presence of mesopores. Fig. 6(a) shows the nano-sized mordenite particles with the incorporation of Ni metal, and the 5 % of Fe metal is randomly distributed on the mordenite. Fig. 6(b) shows an irregular shape of mordenite particles with Ni metal, and the agglomeration is due to the incorporation of 5 % Fe metal. Fig. 6(c–d) illustrates that an increase in the amount of metal incorporation leads to an obscured surface morphology of the mordenite. The dark patches show that the Ni and Fe metals are well dispersed on the mordenite (Groen et al., 2006).

3.6. Temperature-programmed desorption (NH_3-TPD)

The Lewis or Bronsted acid centers and pH of the aided MOR-Fe(5 %)/Ni(5–20 %) catalyst were analysed using NH_3-TPD. The TPD profile of the samples is presented in Fig. 7. The entire MOR-Fe/Ni samples exhibit a non-symmetrical NH_3 desorption peak in the range of 110–600 °C. It is evident that the pinnacle at low temperatures is attributed to the desorption of physisorbed ammonia by weak acid sites. In contrast, the apex at high temperatures is attributed to the desorption of ammonia by strong acid sites, which is in satisfactory correlation with the prior literature. For all the MOR-Fe/Ni samples, the shapes of the NH_3 desorbed in the profile are comparable, though the peaks intensity

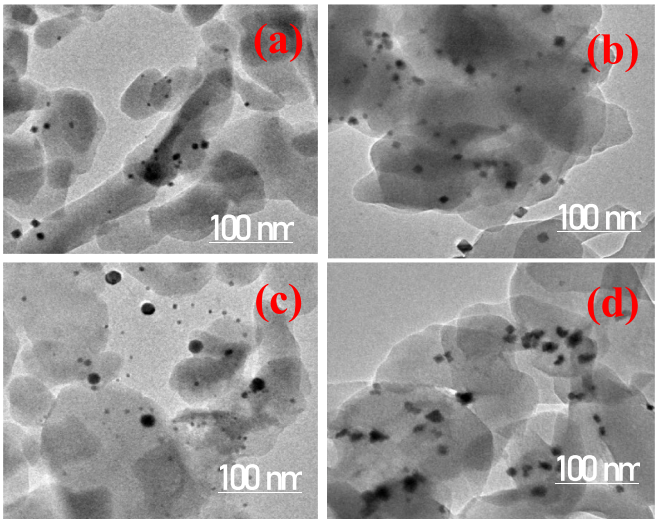

Fig. 6. High Resolution-Transmission Electron Microscopy (HR-TEM) of a)) MOR-Fe(5%)/Ni(5%), b)) MOR-Fe(5%)/Ni(10%), c)) MOR-Fe(5%)/Ni(15%), d)) MOR-Fe(5%)/Ni(20%) samples.

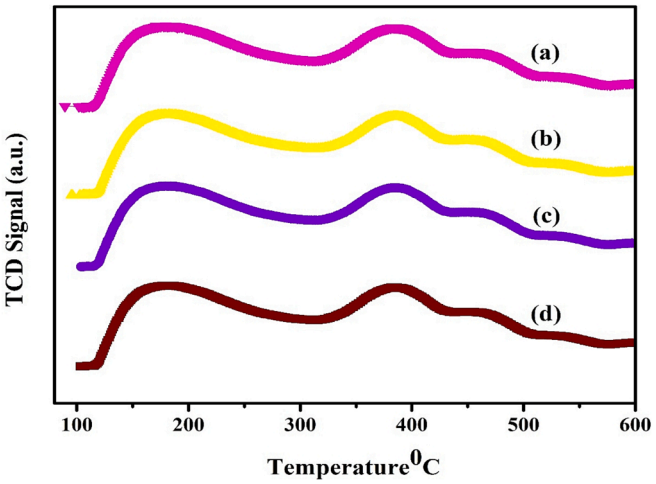

Fig. 7. NH_3-TPD Analysis of of a)) MOR-Fe(5%)/Ni(5%), b)) MOR-Fe(5%)/Ni (10%), c)) MOR-Fe(5%)/Ni(15%), d)) MOR-Fe(5%)/Ni(20%) samples.

declined as the concentration of Fe metal increased. The feeble NH_3 adsorption on the Bronsted acid sites and NH_3 interaction with the Si-OH group should be attributed to the weak acid sites in the range of 110–300 °C apparent in the figure. Strong desorption of NH_3 adsorbed on the acidic Al-OH at the interface, and the doping of Ni and Fe should indeed be attributed to the intense acid sites that appear in the temperature range of 310 to 430 °C. Fig. 7 illustrates that increasing the quantity of Ni increases the acidity and acid strength. Table 1 represents the peak area at low and high temperatures and the total acidity of all the catalysts. The catalyst MOR-Ni (5 %)/Fe (15 %) shows a more excellent acidity of 1.78 mmol/g than the other catalyst. Fig. 7 illustrates that increasing the quantity of Ni increases the acidity and acid strength (Tamizhdurai et al., 2019; Neethu et al., 2021; Das et al., 2020; Gogoi et al., 2021). The acidity of the samples increased in the following order: MOR-Ni(5 %)/Fe(5 %) < MOR-Ni(5 %)/Fe(10 %) < MOR-Ni(5 %)/Fe(20 %) < MOR-Ni(5 %)/Fe(15 %). Thus, catalyst MOR-Ni (5 %)/Fe (15 %) is expected to show higher catalytic activity than the other catalysts.

4. Selective oxidation of veratryl alcohol on MOR-Fe/Ni catalyst

4.1. Catalytic activity and optimization of reaction parameters

The bimetallic loaded onto the supported mordenite was employed for the selective oxidation of VA. On loading the bimetal onto mordenite, the metal Fe is impregnated with a constant molar ratio (5 % wt. %), and the Ni metal is impregnated by varying the molar ratio (5–20 %). The four distinct catalysts are thus: a) MOR-Fe(5 %)/Ni(5 %); b) MOR-Fe(5 %)/Ni(10 %); and c) MOR-Fe(5 %)/Ni(15 %), d) MOR-Fe(5 %)/Ni(20 %), Veratryl alcohol was subjected to the oxidation process in the continuous reactor over the four aforementioned catalysts under controlled reaction circumstances. The reaction conditions are optimised for a diverse range of process variables, including temperature (60–100 °C), $WHSV^{-1}$ (0.1–2.0 hr^{-1}), reaction duration (2–10 hr), pressure (5–20 bar), and solvent, to ascertain which of the four catalysts is the most active and to achieve more excellent veratryl alcohol conversion and veratraldehyde selectivity. The reusability of the catalyst with the highest activity was explored.

4.2. Impact of temperature

The influence of temperature on the conversion and selectivity of the oxidation of VA using MOR-Fe/Ni as a catalyst is illustrated in Fig. 8A &B. Here, the Fe metal loading is kept constant (5 %), and the Ni metal loading is varied by (5–20 %). In the oxidation of VA, the TBHP (1:2) ratio was used as an oxidant. The weighted hourly space velocity was specified as 1.0 h^{-1}, and the oxygen flow rate was retained at 0.1 h^{-1}. Portray selective oxidation of VA using various catalysts at temperatures between 60 and 100 °C. Fig. 8A & B show that the catalysts MOR-Fe (5 %) and Ni (5 %) show very low catalytic activity compared to the others. Whereas the catalyst MOR-Fe (5 %)/Ni (15 %) shows high catalytic activity because the higher percentage of nickel metal shows sufficient adsorption of reactant molecules compared to others. In catalyst (a) MOR-Fe(5 %)/Ni(5 %), the conversion was from 70 to 84 % with a maximum selectivity of 98 %. In catalyst c) MOR-Fe(5 %)/Ni(15 %), at 60–100 °C, the conversion was 84–99 %, and the selectivity was 100 %. The conversion increased from 60 to 90 °C, but at 100 °C, it began to decline considerably. As temperature increases, the rate of the reaction increases, indicating a rise in conversion. At 100 °C, the conversion decreases which is due to the decomposition of TBHP and the formation

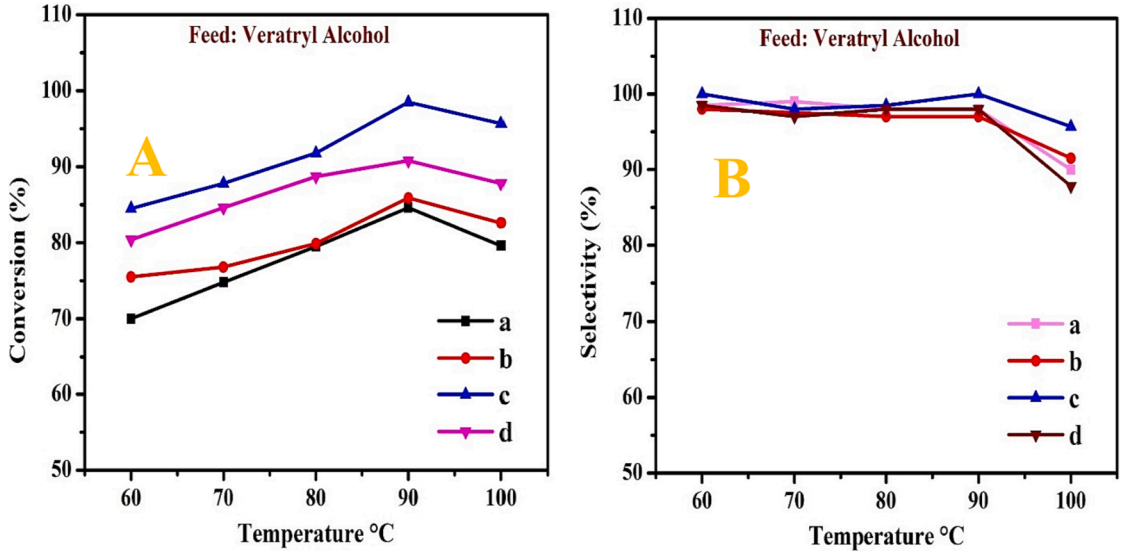

Fig. 8. The effect of temperature on conversion (A) and selectivity (B) of veratryl alcohol. (a) MOR-Fe(5 %)/Ni(5 %), (b) MOR-Fe(5 %)/Ni(10 %), (c) MOR-Fe(5 %)/Ni(15 %), and (d) MOR-Fe(5 %)/Ni(20 %). Reaction condition: catalyst weight = 3.2 g; temperature = 60–90 °C, Pressure = 10 bar, WHSV = 1.0 $h^{-1}$and O_2 flow rate = 1.0 mol h^{-1}.

of a by-product. At 90 °C, both the conversion and selectivity were 100 %. The oxidation of VA is, therefore, best accomplished at a temperature of 90 °C.

4.3. Influence of the pressure

The influence of pressure on the conversion and selectivity of the oxidation of VA using MOR-Fe/Ni as a catalyst in the pressure range of 0 to 20 bar is illustrated in Fig. 9A & B. In the oxidation of VA, TBHP (1:2) was used as an oxidant. The weighted hourly space velocity was specified as 1.0 h^{-1}, and the temperature was maintained at 90 °C. The catalyst MOR-Fe (5 %)/Ni (5 %) shows very low catalytic activity compared to the others. The catalyst MOR-Fe (5 %) / Ni (15 %) shows high catalytic activity because the higher percentage of nickel metal allows for sufficient adsorption of reactant molecules over others. In catalyst a) MOR-Fe (5 %)/Ni (5 %), the conversion was from 78 to 86 %, and the selectivity of the product was about 88 %. In catalyst c) MOR-Fe (5 %)/Ni (15 %), the conversion was from 85 to 96 %, and the selectivity was about 94–99 %. Conversion and selectivity improve as O_2 pressure increases from 5 to 10 bar. From 10 to 20 bar pressure, there was a slight decrease in the conversion and selectivity. The decrease in selectivity indicates that veratric acid is formed during the reaction. Therefore, the catalyst c) MOR-Fe (5 %)/Ni (15 %) shows a maximum conversion of 97 % and a selectivity of 99 % at 10 bar pressure. Therefore, the oxidation of VA can be accomplished with 10 bar O_2 pressure.

4.4. Influence of $WHSV^{-1}$

The influence of $WHSV^{-1}$ on the oxidation of VA was studied using MOR-Fe/Ni as a different catalyst in a molar ratio of Ni-5 to 10 % at a constant pressure of 10 bar and temperature of 90 °C. To accurately predict the WHSV, the catalyst dosage was kept constant while the feed flow range was varied. From Fig. 10A & B, the WHSV range from 0.5 to 2.0 hr^{-1}. The catalysts MOR-Fe (5 %) and Ni (5 %) show very low catalytic activity compared to the others. In catalyst a) MOR-Fe (5 %)/Ni (5 %), the conversion was decreased from 96 % to 79 %, and the selectivity was increased from 79 to 95 %. In catalyst b) MOR-Fe (5 %) / Ni (10 %), the conversion was decreased from 98 to 80 %, and the selectivity was increased from 80 to 96 %. In catalyst c) MOR-Fe (5 %)/Ni (15 %), the conversion was decreased from 100 to 90 %, and the selectivity was increased from 90 to 98 %. In catalyst d) MOR-Fe (5 %) / Ni (20 %), the conversion decreased, and the selectivity increased. As the WHSV increased from 0.5 to 1.0 h^{-1} the conversion decreased slightly and reached an optimum level from 1.0 to 2.0 h^{-1} there was a gradual decrease in the conversion. From 0.5 to 1.0 hr^{-1}, the selectivity reaches an optimum level and decreases further. Among the four catalysts, MOR-Fe/Ni (15 %) shows more catalytic activity than others. At 1.0 hr^{-1}, the conversion and selectivity are much better. Hence, 1.0 hr^{-1} is more effective for the selective oxidation of VA.

4.5. Impact of the time

The impact of time on the selective oxidation of VA using MOR-Fe (5 %)/Ni (5–10 %) as a catalyst at a constant temperature of 90 °C was studied. The catalytic amount was kept constant, and $WHSV^{-1}$ was maintained at 1.0 hr^{-1}. Fig. 11A & B show that the time ranges from 2 to 10 h. In catalyst a) MOR-Fe (5 %)/Ni (5 %), the conversion decreased from 95 to 70 %, and the selectivity was also decreased from 93 to 72 %. In catalyst b) MOR-Fe (5 %)/Ni (10 %), the conversion decreased from 97 to 78 %, and the selectivity was also decreased from 95 to 73 %. The conversion of catalyst c) MOR-Fe (5 %)/Ni (15 %) was reduced from 100 to 90 %, and the selectivity was also reduced from 98 to 90 %. In catalyst d) MOR-Fe (5 %)/Ni (20 %), the conversion decreased from 98 to 83 %, and the selectivity also decreased from 96 to 83 %. As the time increases from 2 to 4 h, the reactant conversion and selectivity will slightly decrease; from 4 to 10 h, there will be a gradual decrease in the percentage of conversion and selectivity. The catalyst, MOR-Fe (5 %)/Ni (15 %), exhibits a maximal conversion of 100 % and a selectivity of 98 % at 2 h. Considering conversion and selectivity, 2 h should be enough for the reaction.

4.6. Influence of the solvent

Solvent influence is much more effective in the selective oxidation of VA using the four different catalysts MOR-Fe/Ni (5–20 %). There are four different types of aprotic solvents, such as CH_3CN (acetonitrile), DMF (dimethyl formamide), $CHCl_3$ (chloroform), and DCM (dichloromethane). The reaction conditions are temperature 90 °C, pressure 10 bar, and time 2 h. Using CH_3CN as a solvent, the four catalysts show conversion > 90 % and selectivity >87 %, as shown in Fig. 12A & B. In DCM, the four catalysts show conversion >74 % and selectivity >66 %. In the DMF, the four catalysts show conversion >67 % and selectivity >67 %. In chloroform, the four catalysts show conversion >51 % and selectivity of 39 %. Among the four different catalysts, MOR-Fe (5 %)

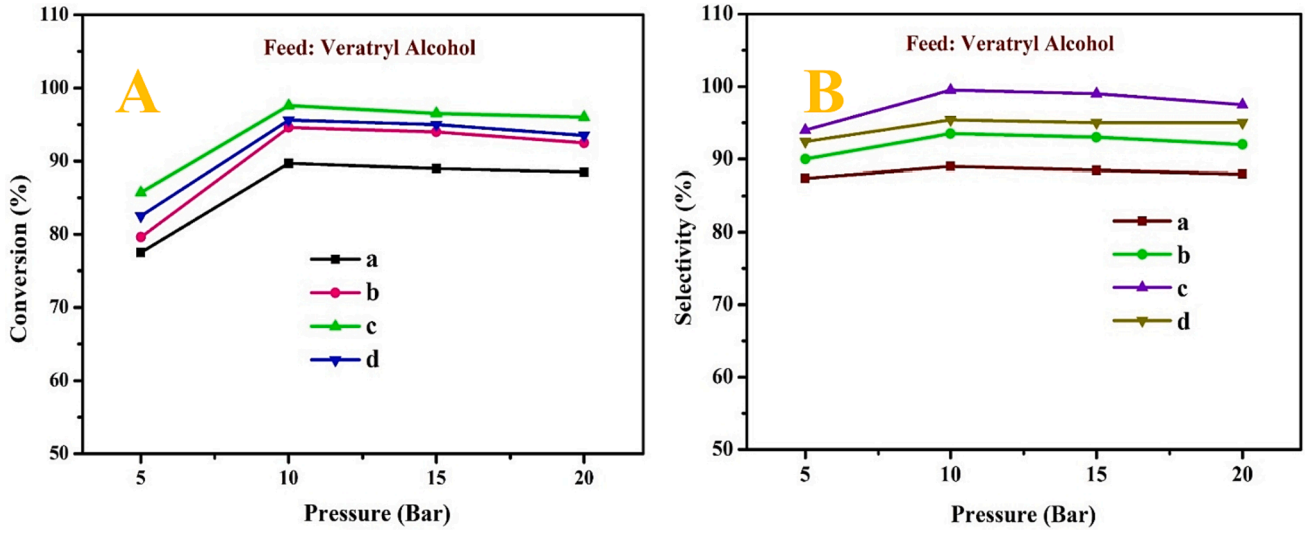

Fig. 9. The effect of pressure on conversion (A) and selectivity (B) of veratryl alcohol, (a) MOR-Fe(5 %)/Ni(5 %), (b) MOR-Fe(5 %)/Ni(10 %), (c) MOR-Fe(5 %)/Ni (15 %), and (d) MOR-Fe(5 %)/Ni(20 %). Reaction condition: catalyst weight = 3.2 g; temperature = 90 °C, Pressure = 5–20 bar WHSV = 1.0 $h^{-1}$and O_2 flow rate = 1.0 mol h^{-1}.

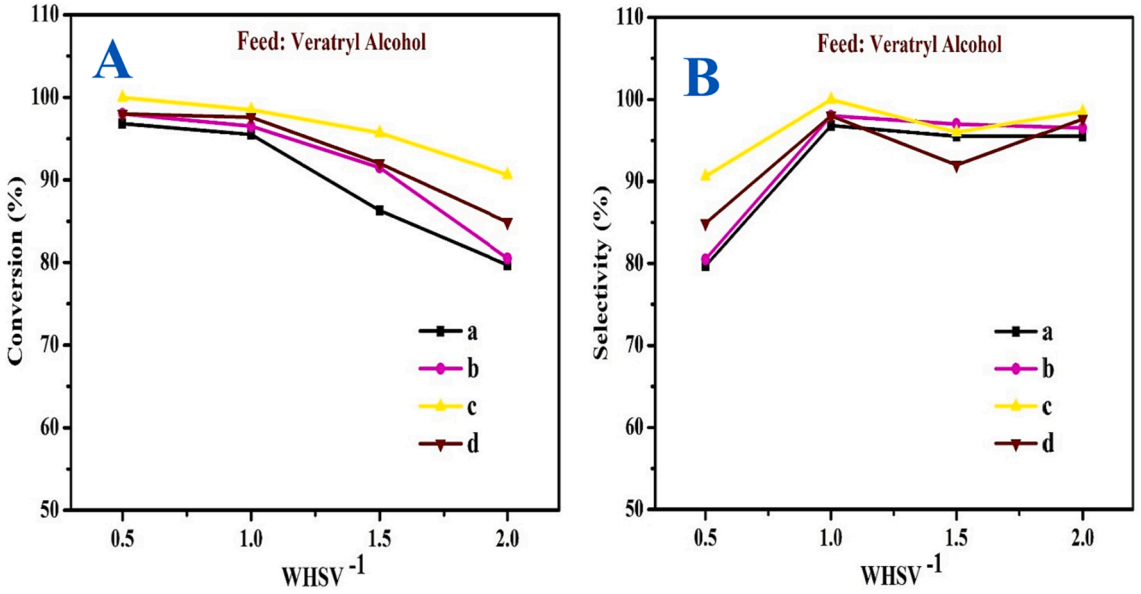

Fig. 10. The effect of WHSV of on conversion (A) and selectivity (B) veratryl alcohol, (a) MOR-Fe(5 %)/Ni(5 %), (b) MOR-Fe(5 %)/Ni(10 %), (c) MOR-Fe(5 %)/Ni (15 %), and (d) MOR-Fe(5 %)/Ni(20 %). Reaction condition: catalyst weight = 3.2 g; temperature = 90 °C, Pressure = 10 bar, WHSV = 0.5–2.0 $h^{-1}$and O_2 flow rate = 1.0 mol h^{-1}.

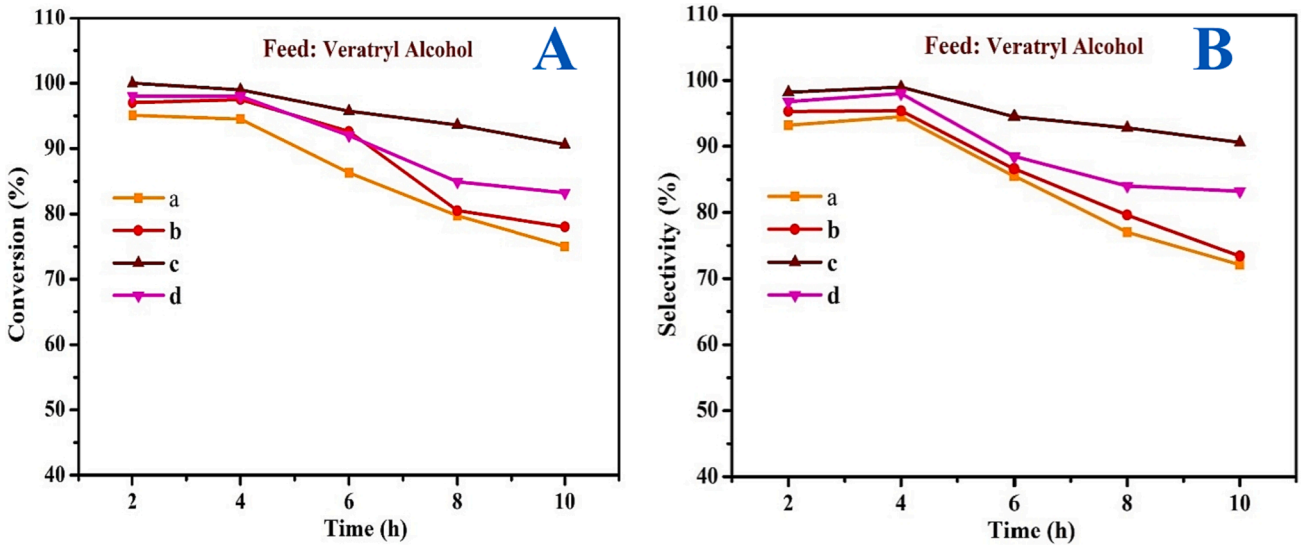

Fig. 11. Effect of time on stream on conversion (A) and selectivity (B) (a) MOR-Fe(5 %)/Ni(5 %), (b) MOR-Fe(5 %)/Ni(10 %), (c) MOR-Fe(5 %)/Ni(15 %), and (d) MOR-Fe(5 %)/Ni(20 %). Reaction condition: catalyst weight = 3.2 g; temperature = 90 °C, WHSV = 1.0 $h^{-1}$and O_2 flow rate = 1.0 mol h^{-1}.

and Ni (15 %) show better conversion (100 %) and selectivity (99 %) in acetonitrile, while the other solvents show minimum conversion and selectivity. This shows that acetonitrile as a solvent is effective for the oxidation of veratryl alcohol. CH_3CN > DCM > DMF > $CHCl_3$.

4.7. Mechanism study

Based on the catalytic studies, it has been observed that MOR-Fe (5 %) and Ni (15 %) exhibit higher activity compared to the other catalysts. The catalyst MOR-Fe (5 %)/Ni (15 %) exhibited a high yield of 99 % in the acetonitrile solvent. According to the observation, a mechanistic pathway is proposed in Fig. 13. Alcohol oxidation is aided by Lewis acid sites. It has been suggested that the ZSM-5 material, after undergoing alkali treatment, shows a comparable process. The oxidation of alcohol is thought to occur due to the presence of Lewis acid sites. During the first step, the solvent acetonitrile easily dissolves with TBHP, leading to the formation of a per-hydroxyl ionic species with NiFe oxide supported on the MOR. The hydroxyl ion interacts with the catalyst supported by the mordenite. The perhydroxyl ion produces a NiFe peroxy complex by selectively interacting with the Fe Lewis acid sites within the mordenite framework. The percentage of Ni on the catalyst was optimised to enhance the presence of sufficient Lewis acid sites. The high catalytic activity of the MOR-Fe(5 %)/Ni(15 %) catalysts can be attributed to the presence of numerous active sites (Yoganandhan et al., 2023; Dhinagaran et al., 2022). During step 2, the NiFe peroxo complex undergoes a reaction with a specific alcohol, resulting in the formation of an intermediate. In step 3, the water molecule is eliminated, leading to the production of veratraldehyde. Finally, at the conclusion of the reaction, the catalyst is regenerated. Veratric acid is produced as a result of excessive oxidation.

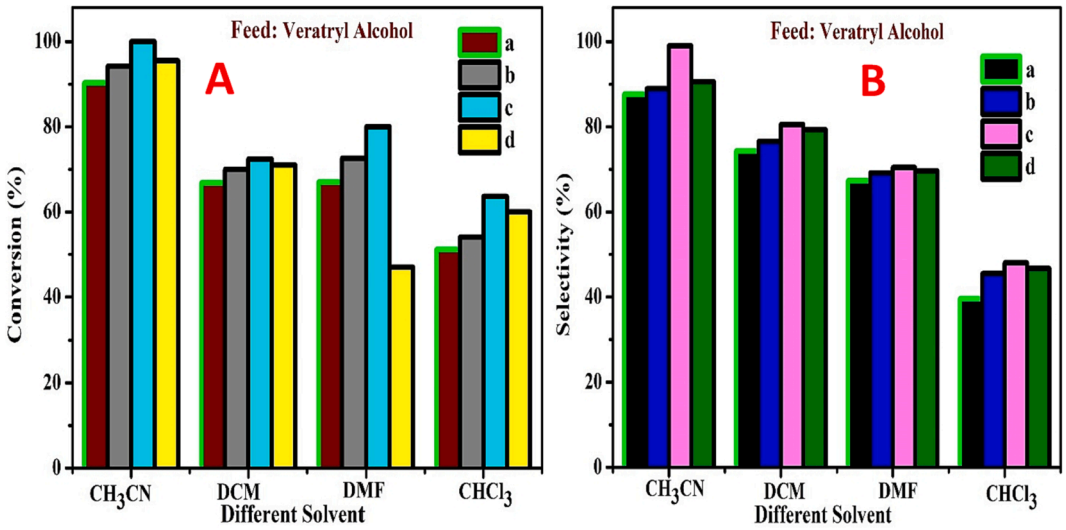

Fig. 12. Effect of solvent on conversion (A) and selectivity (B) of veratryl alcohol (a) MOR-Fe(5 %)/Ni(5 %), (b) MOR-Fe(5 %)/Ni(10 %), (c) MOR-Fe(5 %)/Ni(15 %), and (d) MOR-Fe(5 %)/Ni(20 %). Reaction conditions: H_2O_2 (1:2), temperature (90 °C), solvent 5 mL, catalyst amount 3.2 g, pressure 20 bar.

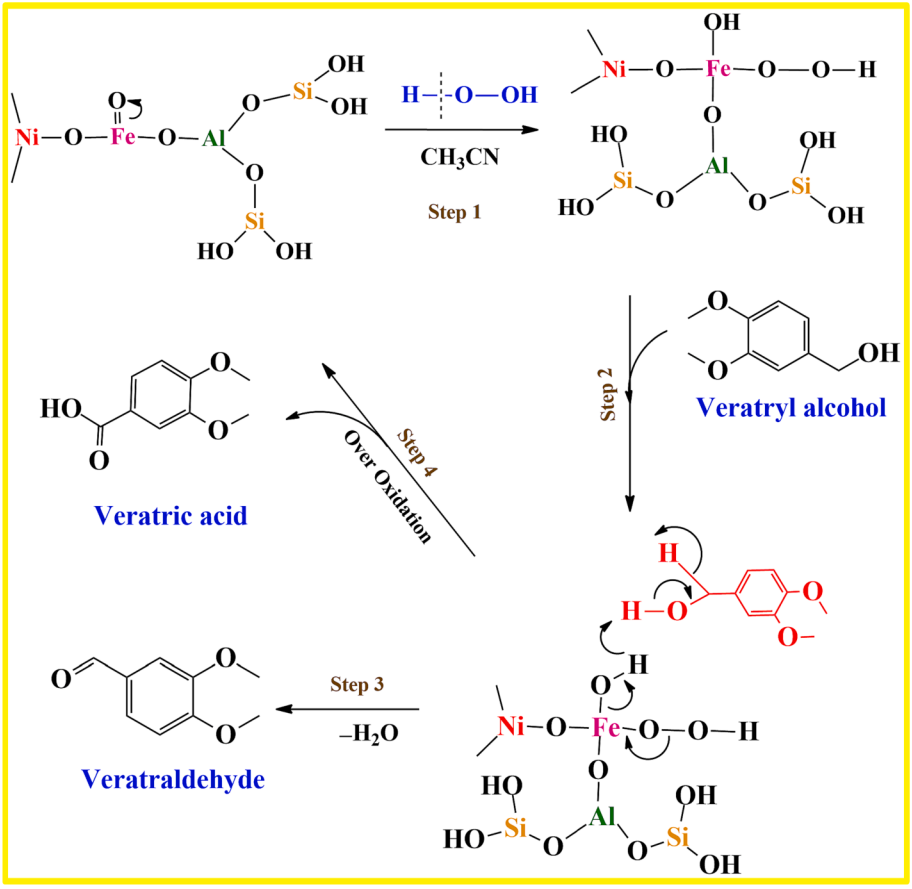

Fig. 13. Proposed reaction mechanism for the oxidation of Veratryl alcohol (VA) to veratraldehyde(VADE).

4.8. Regeneration of the catalyst

Table 2 shows the catalyst stability and recycling performance were studied up to seven cycles. A marginal decrease was observed in conversion for each conversion cycle, and the conversion dropped at 1 % for every cycle. At the end of the 7th cycle, the conversion dropped from 99.5 to 92.4.7 %. Regarding the selectivity studies, the selectivity remained almost the same for the first five cycles and dropped to 1 % for 6th cycle and 3.5 % for the 7th cycle. At the end of the 7th cycle, the selectivity dropped from 100 % to 96.2 %. At the end of seven cycles, the process shows the stability and resilience of the catalyst to deliver an approximate 98 % yield. The relatively high surface area of the catalyst (380 m^2/g) in this continuous process study enabled a high yield compared to the previous batch processing study. During the recycling

Table 2
Catalytic recycles of selective oxidation of veratryl alcohol over the MOR-Fe (5%)/Ni(15) Catalyst.

Recycle	Run-1	Run-2	Run-3	Run-4	Run-5	Run-6	Run-7
Conversion (%)	99.5	99.2	98.9	98.2	97.5	96.5	92.4
Selectivity (%)	100	99.6	98.5	98	97.2	97	96.2

Reaction conditions: Feed: veratryl alcohol = 3 mL, Solvent = TBHP (20 mmol), H_2O_2 = 20 mmol, temperature = 90 °C, Pressure = 10 Bar, time = 4 h, catalyst amount = 3.2 g, Volume (solvent + Reactant) = 6 mL.

study, the temperature was maintained at 90 °C, pressure at 10 bars, WHSV = 1.0 h^{-1}, reaction time 2 h, and the solvent was TBHP.

5. Conclusion

Mesoporous mordenite catalysts with mixed bimetals (Fe/Ni) have been prepared for the selective oxidation of VA to VADE using TBHP as an oxidant and acetonitrile as solvent. It was observed that the selectivity and conversion of VADE depend on the catalytic ratio and solvent. The catalytic chemical reactions take place under mild conditions with a quick process time and high efficiency, and they are also energy efficient and environmentally benign. The higher catalytic selectivity and activity that have been observed are attributed to the modified mesoporous mordenite and the impregnation of metals. we revealed four specific catalyst composition combinations: MOR-Fe/Ni (5 %); MOR-Fe (5 %)/Ni (10 %); MOR-Fe (5 %)/Ni (15 %); and MOR-Fe (5 %)/Ni (20 %). The MOR-Fe (5 %) and Ni (15 %) components of this catalyst have demonstrated remarkable stability and characteristics during testing. These components have also exhibited the highest levels of conversion and selectivity for VA in various catalytic activities. This can be attributed to the reduced particle size, as observed in the TEM image, and the acidity of the catalyst, as indicated by the TPD analysis. With a modified catalyst and a larger mordenite surface, the continuous reactors catalyst (15 %) ratio can produce a maximum yield of more than 98 % under ideal circumstances of high conversion at 90 °C. The final product obtained has a wide range of applications, and therefore, the catalyst MOR-Fe/Ni is anticipated to be of industrial significance because it achieves a higher conversion and selectivity of VA to VADE.

Acknowledgement

The KSU authors would like to extend their sincere appreciation to Researchers Supporting Project number (RSPD2023R779), King Saud University, Riyadh, Saudi Arabia

Appendix A. Supplementary material

Supplementary data to this article can be found online at https://doi.org/10.1016/j.arabjc.2023.105506.

References

Al-Mamoori, A., Alsalbokh, M., Lawson, S., Rownaghi, A.A., Rezaei, F., 2020. Development of bismuth-mordenite adsorbents for iodine capture from off-gas streams. Chem. Eng. J. 391, 123583.
Aloise, A., Marino, A., Dalena, F., Giorgianni, G., Migliori, M., Frusteri, L., Cannilla, C., Bonura, G., Frusteri, F., Giordano, G., 2020. Desilicated ZSM-5 zeolite: catalytic performances assessment in methanol to DME dehydration. Microporous Mesoporous Mater. 302, 110198.
Arumugam, R., Perumal, T., Mangesh, V.L., Kuppusamy, P., Selvaraj, G., Kandhasamy, S., Shanthi, K., 2019. Mg/ $SiO_2eAl_2O_3$ supported nickel catalysts for the production of naphthenic hydrocarbon fuel by hydro-de-oxygenation of eugenol. Int. J. Hydrogen Energy 44, 25607e20.
Aswin, P., Sreenavya, A., Venkatesha, N.J., Ganesh, V., Balamurugan, S., Sakthivel, A., 2022. ChemistrySelect 7, e202202523.
Baruah, M.J., Bora, T.J., Dutta, R., Roy, S., Guha, A.K., Bania, K.K., 2021. Fe (III) superoxide radicals in halloysite nanotubes for visible-light-assisted benzyl alcohol oxidation and oxidative CC coupling of 2-naphthol. Mol. Catal. 515, 111858.
Bogdanov, D.S., Novikov, R.G., Pestsov, O.S., Baranov, D.A., Shelyapina, M.G., Tsyganenko, A.A., Kasatkin, I.A., Kalganov, V.D., Silyukov, O.I., Petranovskii, V., 2021. Formation of admixed phase during microwave-assisted Cu ion exchange in mordenite. Mater. Chem. Phys. 261, 124235.
Cao, X., Wang, R., Wang, K., Gu, Z., Wang, F., 2021. Enhancing the catalytic properties of mordenites via an alkali-acid treatment and by loading nickel-cerium during o-ethyltoluene isomerization. ACS Omega 6, 22688–22699.
Chen, Y., Wang, X., Zhang, L., 2020. Synthesis and catalytic activity of hierarchical NbS-1 zeolites for cyclohexene oxidation. Microporous Mesoporous Mater. 295, 109963.
Das, B., Baruah, M.J., Sharma, M., Sarma, B., Karunakar, G.V., Satyanarayana, L., Roy, S., Bhattacharyya, P.K., Borah, K.K., Bania, K.K., 2020. Self pH regulated iron (II) catalyst for radical free oxidation of benzyl alcohols. Appl. Catal. A 589, 117292.
Dhinagaran, G., Harichandran, G., Suvaitha, S.P., Venkatachalam, K., 2022. Catalytic activity of SBA-15 supported CuO for selective oxidation of veratryl alcohol to veratraldehyde. Mol. Catal. 528.
Dhinagaran, G., Harichandran, G., Suvaitha, S.P., Venkatachalam, K., 2022. Catalytic activity of SBA-15 supported CuO for selective oxidation of veratryl alcohol to veratraldehyde. Mol. Catal. 528, 112454.
Fan, H., Yang, Y., Song, J., Ding, G., Wu, C., Yang, G., Han, B., 2014. One-pot sequential oxidation and aldol-condensation reactions of veratryl alcohol catalyzed by the Ru@ZIF-8 + CuO/basic ionic liquid system. Green Chem. 16, 600–604.
Gillet, S., Aguedo, M., Petitjean, L., Morais, A.R.C., da Costa Lopes, A.M., Łukasik, R.M., Anastas, P.T., 2017. Lignin transformations for high value applications: towards targeted modifications using green chemistry. Green Chem. 19, 4200–4233.
Gogoi, G., Saikia, P., Baruah, M.J., Lee, S., Park, Y.-B., Dutta, R., Bania, K.K., 2021. Mixed valent copper oxide nanocatalyst on Zeolite-Y for mechanochemical oxidation, reduction and C-C bond formation reaction. Microporous Mesoporous Mater. 326, 111392.
Groen, J.C., Moulijn, J.A., Pérez-Ramírez, J., 2006. Desilication: on the controlled generation of mesoporosity in MFI zeolites. J. Mater. Chem. 16, 2121–2131.
Güngör, D., Özen, S., 2021. Development and characterization of clinoptilolite-, mordenite-, and analcime-based geopolymers: a comparative study. Case Stud. Constr. Mater. 15, e00576.
Ibrahim, M., Jalil, A.A., Zakaria, W.F.W., Fatah, N.A.A., Hamid, M.Y.S., Izan, S.M., Setiabudi, H.D., 2021. n-Hexane hydroisomerization over Zr-modified bicontinuous lamellar silica mordenite supported Pt as highly selective catalyst: molecular hydrogen generated protonic acid sites and optimization. Int. J. Hydrogen Energy 46, 4019e35.
Ishimori, H., Suzuki, T., Sakanakura, H., Ishigaki, T., 2020. Establishing soil adsorption testing methods for gaseous mercury and evaluating the distribution coefficients of silica sand, decomposed granite soil, mordenite, and calcium bentonite. Soils Found. 60, 496e504.
Ivanova, I.I., Kasyanov, I.A., Maerle, A.A., Zaikovskii, V.I., 2014. Mechanistic study of zeolites recrystallization into micro-mesoporous materials. Microporous Mesoporous Mater. 189, 163–172.
Jangjou, A., Moqadas, M., Mohsenian, L., Kamyab, H., Chelliapan, S., Alshehery, S., Ali, M.A., et al., 2023. Awareness raising and dealing with methanol poisoning based on effective strategies. Environ. Res. 228, 115886.
KaiyuLi, Z.S., Guilian, L., 2022. Model for analyzing the energy efficiency of hydrogen liquefaction process considering the variation of hydrogen liquefaction ratio and precooling temperature. Int. J. Hydrogen Energy 47, 24194e211.
Kamyab, H., Chellappan, S., Tavakkoli, O., Mesbah, M., Bhutto, J.K., Khademi, T., Alijohani, A.A., 2022. A review on carbon-based molecularly-imprinted polymers (CBMIP) for detection of hazardous pollutants in aqueous solutions. Chemosphere 136471.
Kervinen, K., Lahtinen, P., Repo, T., Svahn, M., Leskelä, M., 2002. The effect of reaction conditions on the oxidation of veratryl alcohol catalyzed by cobalt salen-complexes. Catal. Today 75, 183–188.
Khan, H.W., Khan, M.K., Moniruzzaman, M., Al Mesfer, M.K., Danish, M., Irshad, K., Chelliapan, S., 2023. Evaluating ionic liquids for its potential as eco-friendly solvents for naproxen removal from water sources using COSMO-RS: computational and experimental validation. Environ. Res. 231, 116058.
P.J. Kooyman, Synthesis strategies for the preparation of mixed micro-mesoporous materials. In: A. Gédéon, P. Massiani, F. Babonneau (Eds.) Studies in Surface Science and Catalysis, Elsevier, 2008, pp. 91-96.
Koshti, H., Bandyopadhyay, R., 2023. Liquid-phase benzylation of toluene by benzyl alcohol over micro-mesoporous hierarchical mordenite zeolite. Environ. Sci. Pollut. Res. Int. https://doi.org/10.1007/s11356-023-26777-w. PMID: 37010684.
Kozin, N.Y., Voskov, A.L., Khvan, A.V., Uspenskaya, I.A., 2020. Thermodynamic properties of synthetic zeolite e Mordenite. Thermochim Acta 688, 178600.
Krishnan, P.S., Tamizhdurai, P., Alagarasi, A., Shanthi, K., 2019. Vapour phase hydrodeoxygenation of furfural into fuel grade compounds on NiPMoS catalyst: Synergetic effect of NiP and laponite support. Int. J. Hydrogen Energy 44, 14968–14980.
Larson, T.M., Anderson, A.M., Rich, J.O., 2013. Combinatorial evaluation of laccase-mediator system in the oxidation of veratryl alcohol. Biotechnol. Lett 35, 225–231.
Li, L., Li, J., Cheng, L., Wang, J., Yang, J., 2020. Microwave synthesis of high-quality mordenite membrane by a two-stage varying heating-rate procedure. J. Membr. Sci. 612, 118479.
Li, X., Prins, R., Bokhoven, J., 2009. Synthesis and characterization of mesoporous mordenite. J. Catal. 262, 257–265.

Liu, G., Chen, M., Jin, X., Song, C., He, F., Huang, Q., 2021. Combination of $H_3PW_{12}O_{40}$-TiO_2 catalysts for photo-thermal oxidation of cyclohexene to adipic acid by 30% H_2O_2. J. Environ. Chem. Eng. 9, 105422.
Liu, S., Fang, X., Liu, Y., Liu, H., Ma, X., Zhu, W., Liu, Z., 2020. Dimethyl ether Carbonylation over Mordenite zeolite modified by Alkyimidazolium ions. Catal. Commun. 147, 106161.
Liu, S., Fang, X., Liu, Y., Liu, H., Ma, X., Zhu, W., Liu, Z., 2020. Dimethyl ether Carbonylation over Mordenite zeolite modified by Alkyimidazolium ions. Catal. Commun. 147, 106161.
Liu, Y., Liu, X., Zheng, D., Wang, X., Li, L., Han, L., Liu, S., Liu, S., Yu, S., 2021. Fast synthesis of hierarchical mordenite templated by nanocrystalline cellulose for isomerization of a-Pinene. Ind. Crop Prod. 160, 113139.
Liu, X., Wang, K., Liu, B., Guo, Z., Zhang, C., Lv, Z., 2021. Novel WO_3/SO_4^{2-} ZrO_2eTiO_2 double bridge coordination catalyst hfor oxidation of cyclohexene. J. Solid State Chem. 300, 122239.
Liu, Y., Zheng, D., Li, B., Lyu, Y., Wang, X., Liu, X., Li, L., Yu, S., Liu, X., Yan, Z., 2020. Isomerization of a-pinene with a hierarchical mordenite molecular sieve prepared by the microwave assisted alkaline treatment. Microporous Mesoporous Mater. 299, 110117.
Lorenzo, M., Matteo, P., Gianluigi, S., Basso, L., Liviode, S., 2022. H_2NG environmental-energy-economic effects in hybrid energy systems for building refurbishment in future National Power to Gas scenarios. Int. J. Hydrogen Energy 47, 11289e301.
Ma, Z., Xie, J., Zhang, J., Zhang, W., Zhou, Y., Wang, J., 2016. Microporous Mesoporous Mater. 224, 17–25. https://doi.org/10.1016/j.micromeso.2015.11.007.
McCusker L.B., Baerlocher, C., in Stud. Surf. Sci. Catal., ed. J. Čejka, H. van Bekkum, A. Corma, F. Schüth, Elsevier, 2007, vol. 168, pp. 13–37.
Melián-Rodríguez, M., Saravanamurugan, S., Kegnæs, S., Riisager, A., 2015. Aerobic oxidation of veratryl alcohol to veratraldehyde with heterogeneous ruthenium catalysts. Top. Catal. 58, 1036–1042.
Molleti, J., Yadav, G.D., 2017. Green synthesis of veratraldehyde using potassium promoted lanthanum-magnesium mixed oxide catalyst. Org. Process Res. Dev. 21, 1012–1020.
Narayanan, S., Vijaya, J.J., Sivasanker, S., Alam, M., Tamizhdurai, P., Kennedy, L.J., 2015. Characterization and catalytic reactivity of mordenite – Investigation of selective oxidation of benzyl alcohol. Polyhedron 89, 289–296.
Neethu, P.P., Sreenavya, A., Sakthivel, A., 2021. Molybdate stabilized magnesium-iron hydrotalcite materials: potential catalysts for isoeugenol to vanillin and olefin epoxidation. Appl. Catal. A 623, 118292.
Nie, P., Hu, B., Shang, X., Xie, Z., Huang, M., Liu, J., 2020. Highly efficient water softening by mordenite modified cathode in asymmetric capacitive deionization. Separ Purif Technol 250, 117240.
Paixão, V., Carvalho, A.P., Rocha, J., Fernandes, A., Martins, A., 2010. Modification of MOR by desilication treatments: Structural, textural and acidic characterization. Microporous Mesoporous Mater. 131, 350–357.
Sabarish, R., Unnikrishnan, G., 2019. Synthesis, characterization and evaluations of micro/mesoporous ZSM-5 zeolite using starch as bio template. SN Appl. Sci. 1, 989.
Sahu, P., Ganesh, V., Sakthivel, A., 2019. Oxidation of a ligninderived-model compound: iso-eugenol to vanillin over cerium containing MCM-22. Catal. Commun. https://doi.org/10.1016/j.catcom.2020.106099.
Sakthinathan, S., Tamizhdurai, P., Ramesh, A., Chiu, T.-W., Mangesh, V.L., Veerarajan, S., Shanthi, K., 2020. Platinum incorporated mordenite zeolite modified glassy carbon electrode used for selective electrochemical detection of mercury ions. Microporous Mesoporous Mater. 292, 109770.
Sánchez-López, P., Kotolevich, Y., Miridonov, S., Chávez-Rivas, F., Fuentes, S., Petranovskii, V., 2019. Bimetallic AgFe systems on mordenite: effect of cation deposition order in the NO reduction with C_3H_6/CO. Catalysts 9, 58.
Sánchez-López, P., Kotolevich, Y., Antúnez-García, J., Chávez-Rivas, F., Khramov, E., Berlier, G., Moreno-Ruiz, L., Zubavichus, Y., Petranovskii, V., Fuentes-Moyado, S., et al., 2022. Influence of components deposition order on silver species formation in bimetallic Ag-Fe system supported on mordenite. Catalysts 12, 1453.
Santhana Krishnan, P., Ramya, R., Umasankar, S., Shanthi, K., 2017. Promotional effect of Ni2P on mixed and separated phase MoS2/Al-SBA-15 (10) catalyst for hydrodenitrogenation of ortho-Propylaniline. Microporous Mesoporous Mater. 242, 208–220.
Santhana Krishnan, P., Tamizhdurai, P., Alagarasi, A., Shanthi, K., 2019. Vapour phase hydrodeoxygenation of furfural into fuel grade compounds on NiPMoS catalyst: synergetic effect of NiP and laponite support. Int. J. Hydrogen Energy 44, 14968e80.
Sheng, H., Qian, W., Zhang, H., Zhao, P., Ma, H., Ying, W., 2019. Synthesis of hierarchical porous H-mordenite zeolite for carbonylation of dimethyl ether. Microporous Mesoporous Mater. 295, 109950.
Sheng, H., Qian, W., Zhang, H., Zhao, P., Ma, H., Ying, W., 2020. Synthesis of hierarchical porous H-mordenite zeolite for carbonylation of dimethyl ether. Microporous Mesoporous Mater. 295, 109950.
Stefanidis, S., Kalogiannis, K., Iliopoulou, E.F., Lappas, A.A., Triguero, J.M., Navarro, M. T., Chica, A., Rey, F., 2013. Mesopore-modified mordenites as catalysts for catalytic pyrolysis of biomass and cracking of vacuum gasoil processes. Green Chem. 15, 1647–1658.
Sun, W.-J., Gao, E.-Q., 2020. Sulfonic-functionalized MIL-101 as bifunctional catalyst for cyclohexene oxidation. Mol. Catal. 482, 110746.
Tamizhdurai, P., Sakthinathan, S., Perumal, S.K., Arumugam, R., Annamalai, A., Mangesh, V.L., Subramanian, N., Shanthi, K., Chiu, T.-W., 2018. Highly selective oxidation of benzyl alcohol over Pt-sulphated zirconia supported on SBA-15catalyst by using a high-pressure fixed bed reactor. Polyhedron 155.
Tamizhdurai, P., Ramesh, A., Krishnan, P.S., Narayanan, S., Shanthi, K., Sivasanker, S., 2019. Effect of acidity and porosity changes of dealuminated mordenite on n-pentane, n-hexane and light naphtha isomerization. Microporous Mesoporous Mater. 287, 192e202.
Tamizhdurai, P., Mythily, R., Kavitha, C., Mangesh, V.L., Kumaran, R., Perumal, S.K., Sivaramakrishnan, T., Arul Prasad, A., Govindasamy, T.M., Alothman, A., Ouladsmane, M., 2022. Influence of platinum on mordenite properties and catalytic activity towards cyclohexene epoxidation. Int. J. Hydrogen Energy 48.
Thommes, M., Kaneko, K., Neimark, A.V., Olivier, J.P., Rodriguez-Reinoso, F., Rouquerol, J., Sing, K.S.W., 2015. Physisorption of gases, with special reference to the evaluation of surface area and pore size distribution (IUPAC Technical Report). Pure Appl. Chem. 87, 1051–1069.
Upham, D.C., Orazov, M., Jaramillo, T.F., 2021. Phosphate-passivated mordenite for tandem-catalytic conversion of syngas to ethanol or acetic acid. J. Catal. 399, 132e41.
Vangeel, T., Schutyser, W., Renders, T., Sels, B.F., 2020. Perspective on lignin oxidation: advances, challenges, and future directions. In: Serrano, L., Luque, R., Sels, B.F. (Eds.), Lignin Chemistry. Springer International Publishing, Cham, pp. 53–68.
Verboekend, D., Pérez-Ramírez, J., 2011. Design of hierarchical zeolite catalysts by desilication, Catalysis. Sci. Technol. 1, 879–890.
Verboekend, D., Milina, M., Mitchell, S., Perez-Ramirez, J., 2013. Hierarchical zeolites by desilication: occurrence and catalytic impact of recrystallization and restructuring. Cryst. Growth Des. 13 (11), 5025–5035.
Vu, X.H., Armbruster, U., Martin, A., 2016. Micro/mesoporous zeolitic composites: recent developments in synthesis and catalytic applications. Catalysts 6 (12), 183.
Wahono, S.K., Suwanto, A., Prasetyo, D.J., Hernawan, J.T., Vasilev, K., 2019. Appl. Surf. Sci. 483, 940–946. https://doi.org/10.1016/j.apsusc.2019.04.033.
Wang, X.-s., Li, R.-j., Yu, C.-c., Liu, Y.-x., Xu, C.-m., Lu, C.-x., 2020. Enhanced activity and stability over hierarchical porous mordenite (MOR) for carbonylation of dimethyl ether: influence of mesopores. J. Fuel Chem. Technol. 48, 960e9.
Wang, X., Li, R., Yu, C., Liu, Y., 2021. Study on the reconstruction in the crystallization process of mordenite. Microporous Mesoporous Mater. 311, 110665.
Weng, Y., Qiu, S., Ma, L., Liu, Q., Ding, M., Zhang, Q., Zhang, Q., Wang, T., 2015. Jet-Fuel range hydrocarbons from biomass-derived sorbitol over Ni-HZSM-5/SBA-15 catalyst. Catalysts 5, 2147–2160.
Wu, X., Guo, S., Zhang, J., 2015. Selective oxidation of veratryl alcohol with composites of Au nanoparticles and graphene quantum dots as catalysts. Chem. Communications 51 (29), 6318–6321.
Wu, X., Guo, S., Zhang, J., 2016. Au/graphene quantum dots/ferroferric oxide composites as catalysts for the solvent-free oxidation of alcohols. Mater. Lett. 183, 227–231.
Yoganandhan, N., Tamizhdurai, P., Kavitha, C., Mangesh, V.L., Kumar, N.S., Al Fatesh, A. S., Basivi, P.K., 2023. TiO_2/SO_4/Ni@ SBA-15 catalysts for the selective oxidation of veratryl alcohol to veratraldehyde in a continuous reactor. Mol. Catal. 546, 113250.
Yu, D., Lei, P., Li, Y., Shen, W., Zhong, M., Zhang, J., Guo, S., 2022. Catalytic oxidation of veratryl alcohol derivatives using RuCo/rGO composites. Chem. A Eur. J. 28.
Zakzeski, J., Jongerius, A.L., Weckhuysen, B.M., 2010. Transition metal catalyzed oxidation of Alcell lignin, soda lignin, and lignin model compounds in ionic liquids. Green Chem. 12, 1225–1236.
Zhao, Q., An, J., Wang, X., Li, N., 2021. In-situ hydrogen peroxide synthesis with environmental applications in bioelectrochemical systems: a state-of-the-art review. Int. J. Hydrogen Energy 46 (4), 3204e19.